Effect of Growth Conditions on the Surface Morphology and Defect Density of CS-PVT-Grown 3C-SiC

Manuel Kollmuss,* Francesco La Via, and Peter J. Wellmann*

A systematic approach to determine the most crucial growth parameters and their effect on the surface morphology and defect density of sublimation grown (001) cubic silicon carbide (3C-SiC) is conducted. Close space physical vapor transport (CS-PVT) growth on 3C-SiC and 4° off oriented homoepitaxial chemical vapor deposition (CVD) grown seeding layers is performed. For each growth run, one growth parameter, e.g., temperature, pressure, or N_2 flux is varied, while the other parameters are kept constant. Raman spectroscopy, potassium hydroxide (KOH) etching, as well as optical microscopy and atomic force microscopy (AFM) are used for the sample characterization. Step-flow-controlled growth is observed on all grown samples, while the stacking fault density is generally reduced with respect to the seeding layers. Increased temperature as well as increased pressure leads to roughening of the growth surface attributed to step bunching, while their effect on the stacking fault density seems to be only minor in the analyzed parameter range. Areas of strongly enhanced step bunching are present on all samples, and this effect is more pronounced at higher temperature and pressure. Increased nitrogen doping leads to a decreased stacking fault density but also increases the length of remaining stacking faults. The surface morphology is influenced by N_2 on a macroscopic level rather than on microscopic scale.

1. Introduction

Today cubic silicon carbide (3C-SiC) is mainly grown heteroepitaxially due to lack of suitable seeding material for homoepitaxial growth processes. Two routes are currently under investigation with respect to this topic: on the one hand, growth on hexagonal (4H-SiC and 6H-SiC) substrates using both physical vapor transport (PVT) and chemical vapor deposition (CVD) and on the other hand heteroepitaxial growth on silicon using CVD.[1–3] In the case of the hexagonal SiC substrate, a high supersaturation is applied to intentionally switch the polytype to cubic SiC by 2D nucleation. Based on different stacking sequences of the polytypes, double position boundaries (DPB) will be intrinsically formed if growth steps are present on the substrate.[4] Neudeck et al.[5] have shown that a DPB-free material can be produced using a high-temperature CVD process, if the surface steps on the substrate are removed by a tailored CVD pretreatment prior to the 3C-SiC growth. However, the approach worked only on small scale, since mesas of 10×10 mm^2 need to be prepared on the substrate surface to successfully remove the growth steps. As mentioned before, sublimation processes such as the sublimation epitaxy (SE) can also be used to successfully nucleate cubic SiC on hexagonal substrates using higher off cut angles.[6] Although the higher growth temperatures tend to increase the overall material quality, the formation of DPBs and other defects, as well as sample size limitations still pose major challenges.

For the growth of cubic SiC on silicon, most of the challenges are based on the different material properties between 3C-SiC and Si. The main obstacles are the difference in the coefficient of thermal expansion and the different lattice constants.[7,8] While the latter is responsible for an increased density of defects at the interface between Si and 3C-SiC, the former can lead to a severe wafer bending during the cool-down process after the material deposition. Furthermore, the growth on silicon is limited to the melting point of the substrate material of 1418 °C. To overcome these limitations, Anzalone et al.[9] have developed a multistep CVD process. First a thin 3C-SiC layer is grown heteroepitaxially on Si before the substrate is in situ molten away inside the reactor. Consequently, a homoepitaxial CVD step with the remaining thin 3C layer acting as a seed is performed to increase the material thickness. This process not only allows the use of elevated temperatures but also enables a possible route for the fabrication of seeding material for subsequent homoepitaxial sublimation growth processes such as the close space PVT (CS-PVT). Previous works have already shown the potential of CS-PVT for the growth of high-quality and large-area 3C-SiC materials.[10,11]

M. Kollmuss, P. J. Wellmann
Crystal Growth Lab, Materials Department 6 (i-MEET)
Friedrich-Alexander-Universität Erlangen-Nürnberg (FAU)
Martensstr. 7, D 91058 Erlangen, Germany
E-mail: manuel.kollmuss@fau.de; peter.wellmann@fau.de
F. La Via
CNR-IMM, Sezione di Catania
Stradale Primosole 50, Catania I 95121, Italy

(iD) The ORCID identification number(s) for the author(s) of this article can be found under https://doi.org/10.1002/crat.202300034

**ADVANCED
SCIENCE NEWS**

www.advancedsciencenews.com

CRYSTAL
Research & Technology

www.crt-journal.org

Table 1. Growth conditions of the analyzed crystals.

Growth run	A	B	C	D	E	F	G
Pressure [mbar]	1	0.005	1	3	1	1	1
Temperature [°C]	1965	2010	2010	2010	1980	1980	1985
N_2 flux [sccm]	–	–	–	–	0.5	2.5	5
Growth rate [μm h^{-1}]	90	145	170	140	90	100	95

A various number of growth parameters strongly influence the material quality in sublimation growth of SiC. The quantity of literature on sublimation growth of 3C-SiC, however, is significantly low compared to its hexagonal counterparts, which is mostly based on the low availability of homoepitaxial seeds and, therefore, reduced amount of experimental data. Therefore, in this work, the influence of different growth parameters on the homoepitaxial sublimation growth of 3C-SiC was systematically studied. Optical microscopy, atomic force microscopy (AFM), Raman spectroscopy, and etching in molten potassium hydroxide (KOH) were used to identify correlations between growth parameters and the surface morphology as well as the defect density.

2. Experimental Section

Growth runs were conducted in an inductively heated state-of-the-art PVT reactor using a CS-PVT setup with a hot zone optimized for the sublimation growth of 3C-SiC. Polycrystalline SiC wafers were used as source materials, and the distance between the source and seed was set between 0.75 and 1.2 mm by a graphite spacer. A tantalum foil was placed underneath the source material acting as carbon getter to enhance a more Si-rich gas phase suitable for the stability of 3C-SiC. A more detailed description of the used growth setup can also be found in refs. [1, 2]. All used seeds were cut out of two freestanding 3C-SiC samples with a diameter of 150 mm by laser ablation.[12] The seeds had a thickness of 230 μm, were (001) orientated with a 4° off cut toward [110] and were provided by LPE Epitaxial Technology Center in Catania. They were grown using a homoepitaxial CVD process, described in detail in refs. [9, 13]. To prevent backside sublimation during the growth runs, a carbon containing backside coating was applied to the seeds. The growth temperature was varied between 1960 and 2010 °C (measured at the crucible top); the growth pressure was ranged between 0.5×10^{-3} and 3 mbar, and the growth durations were between 2.5 and 6 h. The resulting samples had a final thickness of 500–950 μm, consisting of the seeding layer and the additionally grown CS-PVT material (340–650 μm). All growth runs were conducted in an Ar atmosphere, and n-type doping was realized by introducing additional N_2 into the reactor. The N_2 flux was set between 1.0% and 9.1% of the Ar flux. **Table 1** gives an overview of the growth parameters.

After the growth runs, the backside coating was stripped with an oxidation process and consequently the samples were dipped in buffered hydrofluoric acid to remove the thin oxide formed during the oxidation. The surface morphology of the samples was characterized with an optical microscope, Axio M1m Imager. Additionally, the profile of macro- and microsteps on the surface was analyzed using a Lext OLS 4000 Olympus laser microscope (LSM) operating at a wavelength of 790 nm as well as

a Bruker Dimension Icon atomic force microscope operating in "Scanasyst" mode. Raman spectroscopy was conducted using a Horiba LabRAM HR Evolution confocal Raman microscope in backscattered geometry, operating with a diode-pumped solid-state laser (laser power = 3.2 mW), a 50× magnification lens and an optical grating of 1800 gr mm^{-1}. The laser wavelength was 532 nm resulting in a penetration depth of $\approx$300 μm based on the absorption coefficient of 3C-SiC. Raman measurements were used to determine the overall crystalline quality based on the full width at half maximum (FWHM) of the transversal optical (TO) mode. This mode is forbidden in a perfect (001) oriented 3C-SiC. However, structural defects as well as stress will make the mode visible, allowing for an evaluation of the material quality. Additionally, the concentration of free charge carriers was approximated based on the longitudinal optical (LO) mode. While the mode is located at a Raman shift of 972 cm^{-1} for undoped 3C-SiC, the peak position as well as the peak shape will change due to doping with N_2, which can be used for the determination of the doping level.[14] Note that impurities acting as p-type dopants such as B and Al, which can be present in the grown materials in the low 10^{17} cm^{-3} range, will compensate the charge carriers introduced by N_2 doping, resulting in a slight underestimation of the doping level by Raman measurements. However, since the measured carrier concentrations were in the order of 10^{18}–10^{19} cm^{-3} this effect could be neglected. For defect etching the samples were polished and afterward etched in molten KOH using a self-developed KOH-etching setup.[15] All samples were etched at 400 °C for 2 h and cleaned with hydrochloric acid to remove the KOH residuals from the sample surface. Subsequently, the stacking fault (SF) density for defects with a length of >2 μm was determined from optical microscope images.

3. Results and Discussion

3.1. Influence of Growth Temperature

The first growth series (including crystals A, C, and E) was carried out at a constant pressure of 1 mbar and different temperatures to investigate the influence of the growth temperature and growth rate, respectively. Note that in CS-PVT, the growth rate is strongly connected to the growth temperature if the pressure and the seed-to-source distance are kept constant.[16] While crystal E was intentionally doped, the carrier concentration for all three growth runs was in the range of low to mid 10^{18} cm^{-3}. Unintentional doping of crystals during the CS-PVT growth will occur due to two mechanisms. On the one hand, nitrogen is absorbed in the used carbon isolations during opening and closure of the growth reactor and will desorb during the high-temperature growth. On the other hand, nitrogen will be released from the used polycrystalline source material. For the first growth series, no effects were found that could be attributed to the doping alone, but rather to the different growth temperatures.

Figure 1 shows an AFM measurement on the surface of crystal A and the corresponding histogram for the step height distribution over the whole sample. The surface exhibits a step flow consisting of microsteps mainly aligned in the [110] direction, which fits the off-cut direction of the seeding layers. Locally small deviation from the distinct crystallographic orientation can be observed. Underneath the microsteps, a macrostep structure can
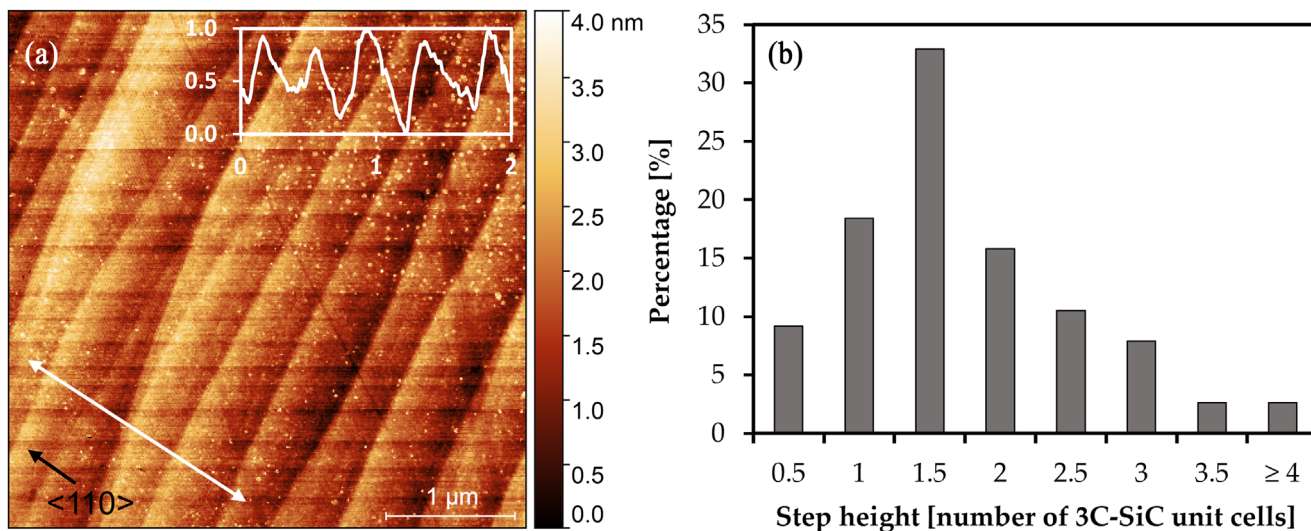
2300034 (2 of 10)

**ADVANCED
SCIENCE NEWS**

www.advancedsciencenews.com

CRYSTAL
Research&Technology

www.crt-journal.org

Figure 1. a) AFM image from the as grown surface of crystal A showing the step flow pattern present on the surface (step flow direction indicated) and corresponding line profile measurement (white line and inset). The y-axis of the inset is in nanometers while the x-axis is in micrometers. b) Histogram of step height distribution measured at multiple spots on the surface of crystal A. The unit of the step heights on the x-axis corresponds to the number of 3C-SiC unit cell heights ($\alpha = 0.436$ nm).

be found similar to the observation in.[10] Additional protrusion defects can be found on the surface. These defects are already present in the seeding layer and enlarged with increasing thickness of the grown crystals.[10,17] The width of the microsteps ranges between 50 and 600 nm, and the step heights are mostly between 0.22 and 0.88 nm (see Figure 1b). The step heights correspond well to the height of half the unit cell of 3C-SiC (0.218 nm) up to two unit cells. Additionally, single steps with heights up to 2 nm are present, concluding that slight step bunching occurs during the CS-PVT growth. The step flow is mostly constant resulting in a smooth surface roughness of 0.5 nm measured by AFM (5×5 μm^2).

Areas with enhanced step bunching (see **Figure 2**)—in the following referred to as macrobunching (MB)—are detectable on the surface as well. In these areas, the step heights and widths increase up to a few 100 nm and 10 μm, respectively. The orientation of this structures follows the [110] step flow direction but also alignments rotated by 90° can be found, which correspond to the [1−10] and [−110] directions, respectively. MBs are mostly observed near protrusion defects, which strongly interact with the step flow during the growth process but can also be found elsewhere on the surface, often paired with the appearances of SFs at the edges of the bunched area (see Figure 2). The SFs, which are aligned in the (111) plane, are perpendicular to the step flow direction at the growth front. We believe that the SF present near the MBs could act as an obstacle at which the step flow is hampered. Meanwhile, at the edges of the SFs, the bunched steps circumvent the defect faster, which results in a chance of the step flow direction in this area, comparable to the formation of triangular defects in step-flow-controlled epitaxy of hexagonal SiC. Consequently, MBs can also be observed at 90° rotated to the growth direction, which is not seen isolated but always at the edges of MBs aligned in step flow orientation. Eventually, the step flow can overcome the defect completely, resulting in an undisturbed step flow behind the SF. It should be noted

that this bunching behavior is not observed at every SF present. Therefore, further research would be necessary to clarify which effects influence if bunching occurs at SFs or not.

Figure 2 shows the described behavior on the surface of crystal E. MBs along the [110] as well as [1−10] direction are visible, while SFs at the edges of the MBs can be seen (yellow guiding lines). The subscript letters for the SFs indicate the termination of the defects. The clearly visible shifts (best seen in relation to the guiding line) for the SFs in horizontal and vertical directions before and after the KOH etching are based on the orientation of the {111} planes, which are ≈45° tilted with respect to both the (001) and {110} planes. During the polishing process, at least a few 10 μm of materials are removed. Therefore, the position at which the defects reach the surface is changed compared to the no-processed surface.

For increased growth temperatures and thus increased growth rates, a roughening of the crystal surface can be observed. The surface roughness increased from 0.5 nm at 1965 °C to 0.7 nm at 1980 °C and 3.4 nm at 2010 °C, respectively, which can be attributed to an enhanced step bunching. Although an ordered step flow is still present at the growth front, the number of bunched steps and their height increases, leading to a rougher surface. A similar trend was reported by Camarda et al. for the step-flow-controlled deposition of both cubic and hexagonal SiC.[18] Consequently, also the dimensions of the MBs increased for higher growth rates. Values up to 3 μm could be measured for the heights of MBs at 2010 °C and the width increased to maximum values of up to 70 μm (see **Figure 3**).

While the step structure and the surface morphology are influenced by the growth temperature, no trend of the FWHM of the Raman TO mode or the SF density with respect to the growth temperature was observed (see **Figure 4**). Figure 4a shows a representative Raman spectrum obtained from the grown samples. Besides the two characteristic modes for 3C-SiC, no further peaks are visible. The values for the FWHM of the TO mode
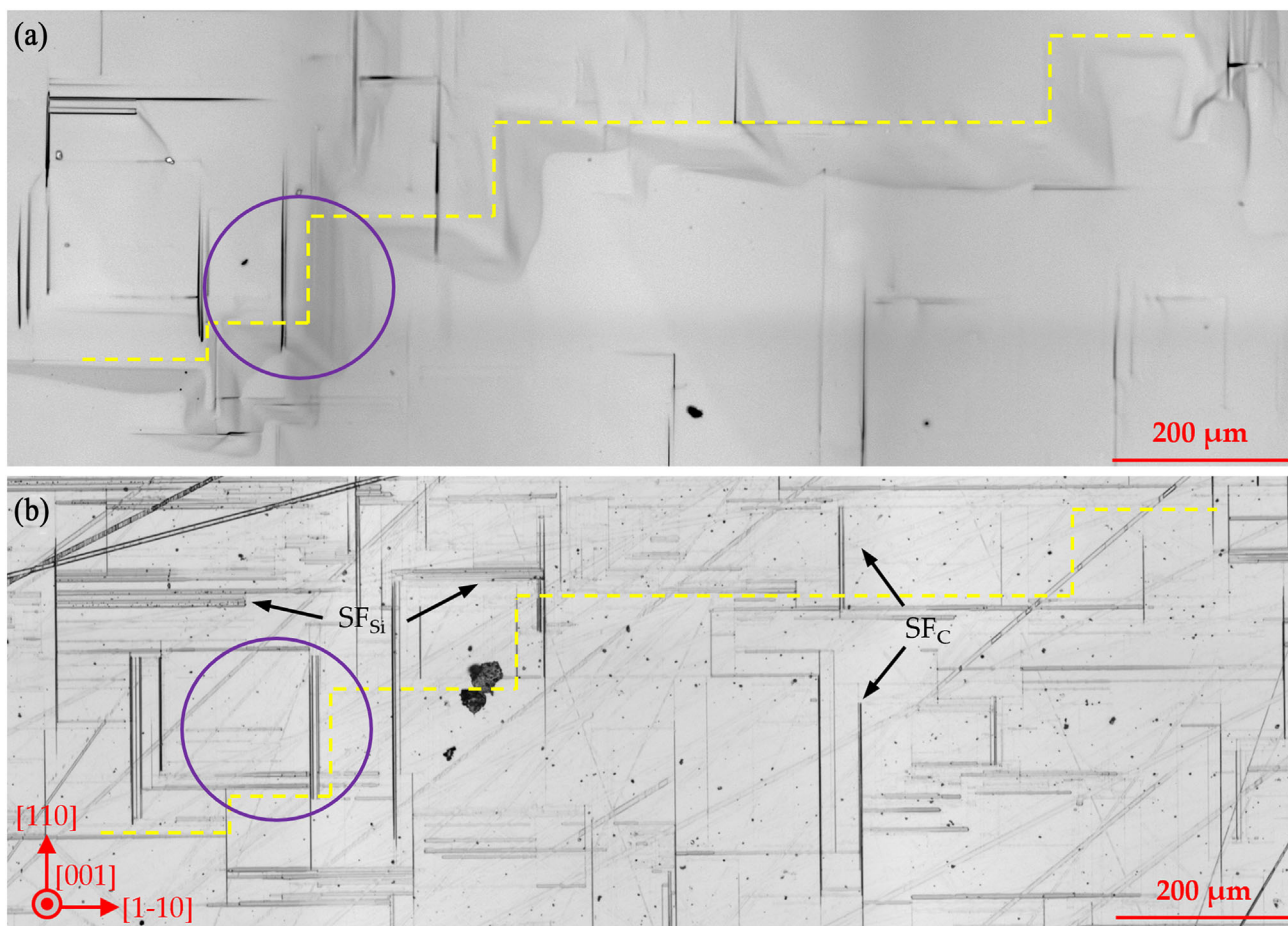
**ADVANCED
SCIENCE NEWS**

www.advancedsciencenews.com

CRYSTAL
Research & Technology

www.crt-journal.org

Figure 2. Comparison of a) the surface of crystal E directly after the growth run with clearly visible macrobunching (MB) (yellow guiding line) and b) the surface appearance after KOH etching. At the edges of the MB SFs can be seen. The noticeable shift of the horizontal and vertical aligned SFs before and after the KOH etching is based on the orientation of the {111} planes which are ≈45° tilted with respect to both the (001) and {110} planes. The subscript letters for the SFs indicate the termination of the defects. The purple marking shows MBs in the [110] and [1−10] directions. If at the edge of an MB oriented in the [110] step flow direction a second SF aligned in (−111) or (1−11) is present, the redirected step flow at the edge of the first MB could undergo enhanced bunching in the locally new growth step direction.
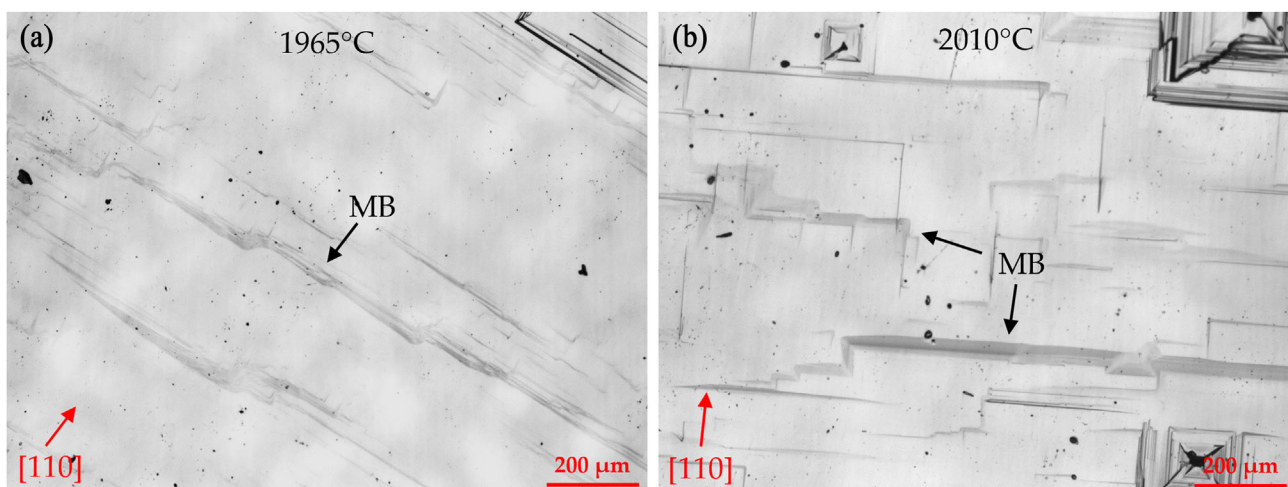

Figure 3. Optical microscope images of as grown surfaces of a) crystal A and b) crystal C showing MBs. The size of the MBs increases with increasing temperature. The growth temperature is indicated in the upper middle part, and the step flow direction is indicted at the bottom left corner.
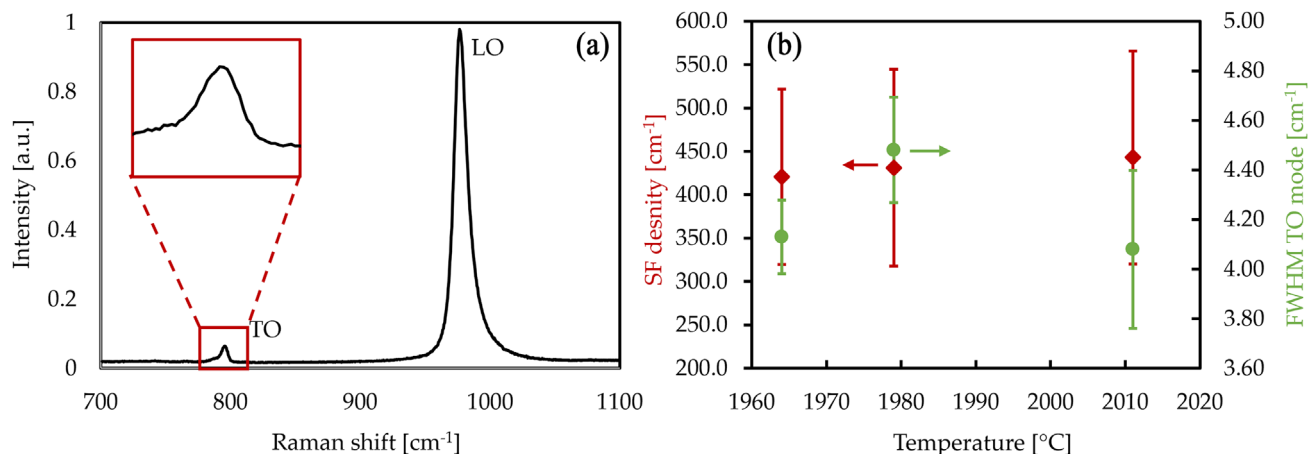
ADVANCED
SCIENCE NEWS

www.advancedsciencenews.com

CRYSTAL
Research&Technology

www.crt-journal.org

Figure 4. a) Typical Raman spectrum for the measurement of 3C-SiC grown by CS-PVT. Besides the polytype specific TO and LO modes no further peaks are observable. b) SF density (red) and FWHM of the TO mode (green) for different growth temperatures of CS-PVT grown 3C-SiC.
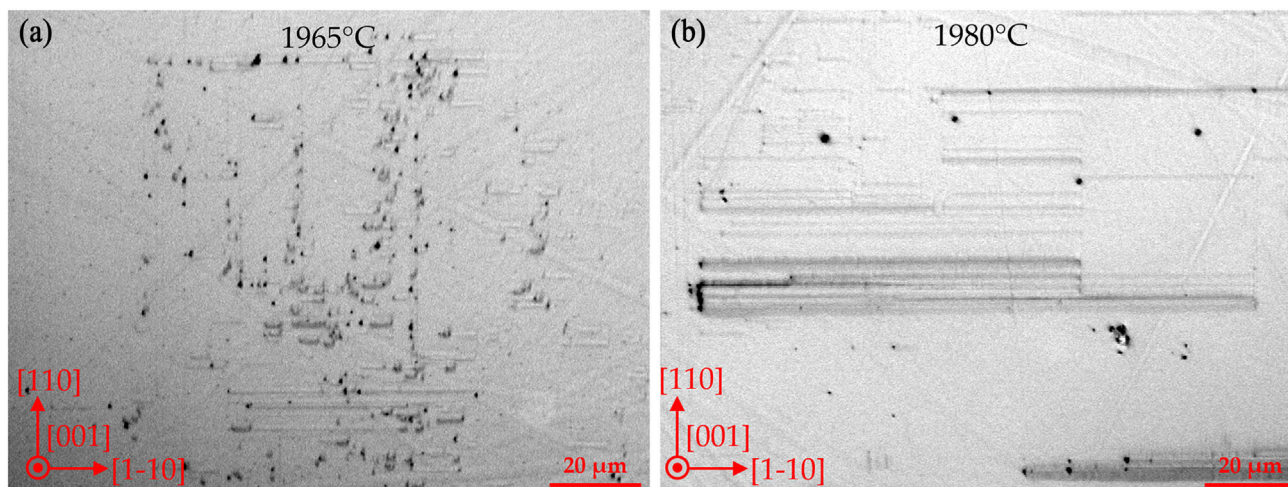

Figure 5. Optical microscope images after KOH etching of a) crystal A and b) crystal E. A preferred orientation of the Si-face SFs aligned in the (111) plane is visible (SFs aligned in (−1−11) are suppressed by the step flow direction). For increased temperature, the average length of the SFs is increased. The growth temperature is indicated in the upper middle part and the crystallographic directions are indicted at the bottom left corner.

are in the range of (4.1–4.5) $\pm$ 0.3 cm^{-1} (see Figure 4b), indicating a constant material quality for all grown crystals. The SF density is in the range of (400–450) $\pm$ 150 cm^{-1}, compared to $\approx$1000 $\pm$ 200 cm^{-1} for the used seeding layers. It is reported in literature that sublimation growth processes can help to significantly decrease the defect density in cubic silicon carbide.[19] Meanwhile, a decreased SF density as well as decreased defect length is predicted at lower growth temperatures for (001)-oriented 3C-SiC.[9] While the latter can be observed in the grown samples (see **Figure 5**), no difference in the SF density can be found, which is in contrast with the findings reported by Schoeler et al.[19] This may be attributed to the already lower overall defect densities in our material.

SFs in 3C-SiC are alignment in four equivalent {111} planes. The Si-face SFs expand during the continuous growth, while the C-face SFs are reduced base on self-vanishing.[20] For the growth of 3C-SiC with an off cut toward [110] the propagation of SFs lying in the (111) plane is favored, while the expansion in (−1−11)

opposite to the step flow direction is suppressed. Based on this behavior, a predominant alignment of the defects at the surface is expected, which can be observed accordingly on all grown samples after KOH etching. However, some defects are also aligned with a 90° rotation on the surface and can be attributed to remaining C-face SFs, which are aligned along the (−111) and (1−11) orientations. The presence of this defects could increase bunching of the macrosteps along the [1−10] and [−110] directions, enhancing the formation of MBs aligned at 90° rotated to the regular step flow. As described before, the interaction between the step flow and the SFs in the [110] growth direction could lead to a local change of the step flow direction at the SF edges. If a second SF aligned in (−111) or (1−11) orientation is present at the edge of the first SF, the redirected step flow could undergo enhanced bunching in the locally new growth step direction as well. This effect was observed in all grown samples in this study and is also visible in Figure 2 (highlighted in purple). It should be noted that the described formation mechanism of MBs is by no means a
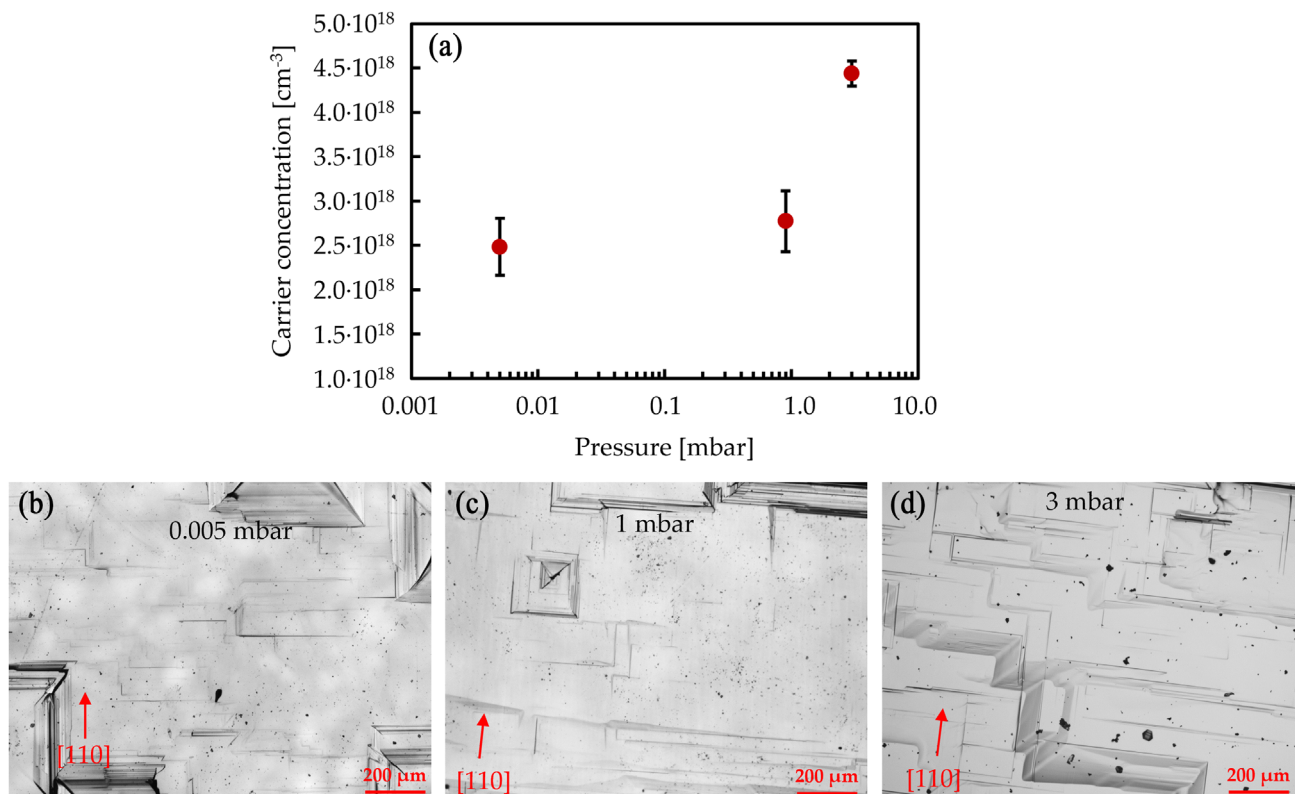
2300034 (5 of 10)

Figure 6. a) Incorporation of N_2 versus growth pressure at fixed growth temperature of 2010 °C during CS-PVT. An increase of the carrier concentration for the growth at higher pressure is observable. This effect is mainly based on the higher partial pressure of nitrogen at higher growth pressure. b–d) Microscope image of the growth surface of crystals B–D grown at different inert gas pressures. The pressure is indicated at the top of the microscope image. Increased dimensions of MBs can be found on crystal D (3 mbar) compared to the growth at lower pressure.

definite statement on their physical origin but rather a theory based on the observation made.

3.2. Influence of Pressure

The growth of crystals B, C, and D was carried out at a constant temperature of 2010 °C without intentional doping but with varied pressures. For crystals B and C, the growth pressures were 0.005 and 1 mbar (set in the reactor), respectively, and the carrier concentrations calculated from Raman measurements were $2.5 \bullet \times 10^{18}$ and 2.8×10^{18} cm^{-3}, respectively (see **Figure 6**). Crystal C exhibits slightly higher growth rates of 170 µm h^{-1} compared to 145 µm h^{-1} for crystal B. For both crystals, a similar surface morphology characterized with an ordered step structure consisting of bunched steps was found. Some of the steps reach a height of up to 20 biatomic layers, which indicates that strong step bunching attributed to the high growth temperature of 2010 °C occurs. The overall surface roughness values were 2.0 and 3.4 nm for crystals B and C, respectively. The MBs had similar widths and heights of up to 70 and 3 µm for both samples. The SF density obtained after KOH etching was in the range of 400–450 cm^{-1}, and no significant difference in the SF length could be obtained.

Although both crystals were grown at different pressures, the actual pressure inside the crucible is determined by the temperature-dependent partial pressures of the gas species con-

tributing to the SiC growth (Si, Si_2C, and SiC_2). For the growth temperature of 2010 °C (measured at the crucible top) the actual temperature at the top of the source material is 2056 °C resulting in a total pressure of 1.3 mbar of the SiC gas species.[21] Therefore, the pressure present between source and seed exceeds the pressure set during the growth of crystal B (0.005 mbar) and crystal C (1 mbar). This means that the growth conditions for both crystals were nearly equal explaining the similar results with respect to surface morphology and defect density.

While the growth pressure was higher for crystal D, the growth rate (140 µm h^{-1}) is similar compared to crystals B (145 µm h^{-1}) and C (170 µm h^{-1}). This was achieved by reducing the seed-to-source distance from 1 to 0.75 mm, eliminating effects due to the growth rate variation. For crystal D, an increased N_2 incorporation was detected with 4.5×10^{18} cm^{-3} compared to crystals B and C (see Figure 6). All three growth runs were doped unintentionally, and the doping level of the used source material can be considered constant. The higher growth pressure of crystal D (3 mbar) exceeds the pressure contributed by the reactive SiC gas species. While the concentration of reactive gas species is determined by the temperatures present above the source, N_2 (and Ar) diffuses into the crucible and inside the crucible only based on the concentration gradient. If no changes to the gas phase composition are made, an increased system pressure (realized by a decreased extraction rate of the used vacuum pump) will also lead to an increased partial pressure of N_2. Thereby the available

**ADVANCED
SCIENCE NEWS**

www.advancedsciencenews.com

CRYSTAL
Research&Technology
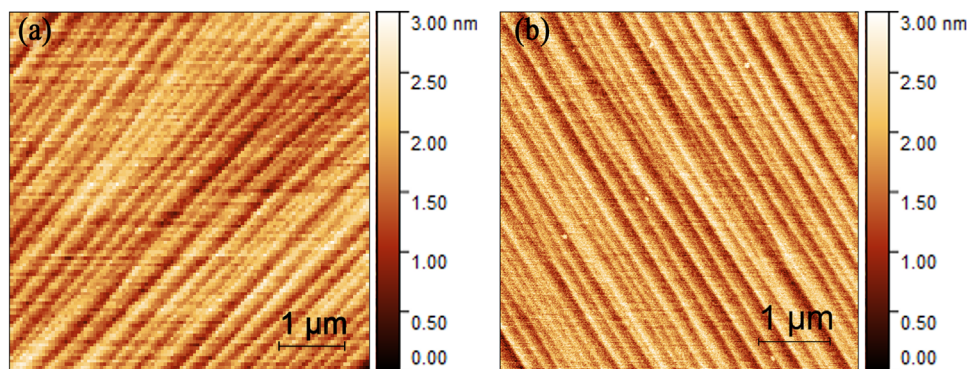
www.crt-journal.org

Figure 7. AFM image of step flow on the surface of a) medium-doped crystal E and b) high-doped crystal G. In both cases, the dimensions of the microsteps are similar with heights of half a unit cell up to 2.5 unit cells. The results are similar to the morphology shown in Figure 1 for a low-doped crystal.

amount of N_2 species in the crucible, for incorporation into the growing crystal, is enhanced, resulting in the higher doping level of crystal D compared to crystals B and C. A similar effect was observed for the sublimation growth of hexagonal SiC polytypes as well as for the CVD growth of cubic SiC.[22,23]

The overall roughness of crystal D is comparable to crystals B and C with 3.2 nm, featuring a step flow structure consisting of bunched steps. However, the dimensions of the MBs as well as their amount visible at the surface are increased. For crystal D, heights up to 5 µm and widths up to 100 µm could be observed for MBs, compared to 3 and 70 µm for the lower growth pressures, respectively. Increased step bunching at higher growth pressures was also reported for the PVT growth of 4H-SiC.[24] However, this is more of an indirect effect based on a change in the C/Si ratio with an increased growth pressure. The reactive gas species attributing to the SiC growth, namely Si, SiC_2, and Si_2C, have different molecular sizes and, therefore, different transport properties. For more detailed discussion regarding the gas-phase composition the following literature is recommended.[21,25] The reactive gas species will sublime from the source based on their temperature-dependent partial pressures and are transported to the seed crystal by diffusion and Stefan flow.[26] While Si has the highest diffusion coefficient, SiC_2 has a lower one.[27] For an increased growth pressure, the mass transport between the source and seed is increasingly dominated by diffusion and consequently is slowed down. This effect should be most significant for the slowest diffusing species SiC_2 thus leading to a reduced C/Si ratio at the seed. The more Si-rich growth conditions favor step bunching based on dissolution of crystallographic unstable steps by the excess Si and the expansion of crystallographic stable steps. Although this observation was made on 4H-SiC, the same effect may apply as an explanation for the observed differences in the surface morphology for increased growth pressure in our study. Furthermore, the lower C/Si ratio additionally explains the increased N_2 concentration observed for crystal D. During SiC growth, nitrogen will be incorporated into a C lattice side based on the side competition effect between C and N atoms.[28] For the reduced availability of C because of reduced C/Si ratio at increased growth pressures, an increased incorporation of N_2 into the growing crystal should occur.

3.3. Influence of N_2 Doping

The last growth series (crystals E–G) focused on the impact of N_2 doping during the CS-PVT growth while crystal A is used as a nominal low-doped (only unintentionally doped) reference. The N_2 flux was modified while the overall pressure and temperature were kept constant for the growth runs. **Figure 7** shows the step flow on the surface of crystal E ($n = 4.5 \times 10^{18}$ cm^{-3}) and crystal G ($n = 1.8 \times 10^{19}$ cm^{-3}). While the doping level is different, no significant changes in the microsurface structure are visible. The microsteps have a usual height between 0.2 and up to 2.2 nm with most of the steps being in the range of 0.2–1.0 nm, which are comparable to the values found in the low-doped crystal A ($n = 1.2 \times 10^{18}$ cm^{-3}). The steps width ranges between 50 and 400 nm, which is slightly lower than the widths measured on crystal A. The results of the AFM measurements indicate that N_2 does not seem to enhance step bunching at least at the microscopic scale during CS-PVT of 3C-SiC. This finding is further supported by the measurement of the surface roughness, which is similar for all crystals of this growth series and is in the range of 0.5–0.8 nm (see **Figure 8**a).

While the N_2 doping seems to have no significant influence on the surface morphology with respect to the microsteps, changes in the macroscopic surface appearance can be observed. Both the width and the height of MBs increase for higher doping levels (see Figure 8a). For low-doped samples, the height and width of the MBs are in the range of a few 100 nm to 1.5 µm and 10–40 µm, respectively. Meanwhile these values increase up to 3 and 100 µm for the highest doped samples, indicating an enhanced step bunching at the macroscale. Nitrogen-induced step bunching could be observed for the PVT and CVD growth of 4H-SiC in literature.[29,30] It is often explained by the interaction between the change of the asymmetric step kinetics influenced by the adsorbed N_2 at the surface and the repulsive step interaction. At this stage, it is not clear whether a similar effect is responsible for the observed macrostep bunching of the nitrogen-doped 3C-SiC samples.

Besides the morphological influence, the effects of the N_2 doping on the material quality were also analyzed. The CS-PVT growth overall led to a reduced SF density compared to the intrinsic seeding layers and a trend toward reduced SF density
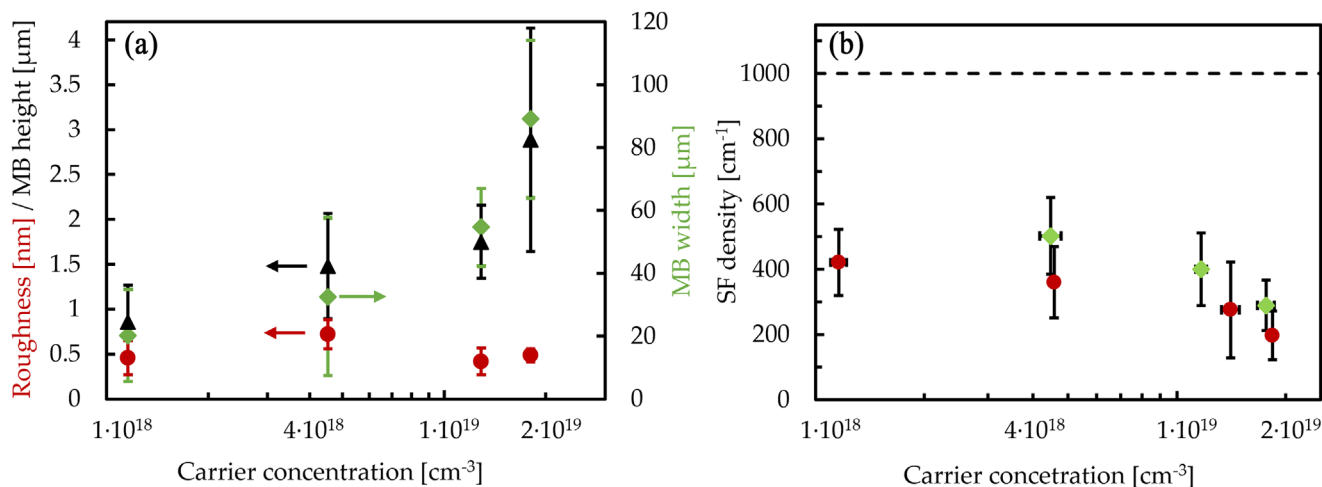
**ADVANCED
SCIENCE NEWS**

www.advancedsciencenews.com

CRYSTAL
Research&Technology

www.crt-journal.org

Figure 8. a) Effect of N_2 doping on the surface morphology of CS-PVT grown 3C-SiC at otherwise constant growth conditions. The surface roughness measured on a 5×5 μm^2 area (red) shows a constant value, while the width (green) and height (black) of the MBs increase with increasing doping levels. All values are average values. b) SF density versus carrier concentration for nitrogen-doped crystals A, E, F, and G (red) grown at constant pressure and temperature. The black dashed line indicates the value for the used seeding layers. A decrease of the SF density with increasing N_2 doping is visible while the overall density is lower for the CS-PVT grown crystals compared to the seeding layer. A second growth series (green) grown under similar conditions, but on a different seeding layer, shows the same trend.

with increased doping levels is observable. In Figure 8b, the doping concentration-dependent SF density for the grown crystals is plotted. The doping level was measured at multiple spots on the sample surface, and the plotted values are average values with error bars for the SF density and the N_2 doping level. No significant deviation of the carrier concentration was observed over the single samples, indicating a homogeneous doping. The measured SF density for the lowest doped crystal A is 400 ± 100 cm^{-1}, while for the highest doped crystal G values of 200 ± 100 cm^{-1} were observed. The evolution of the SF density shows the same trend as for the growth of 3C-SiC using CVD.[31] N_2 is reported to increase the formation energy of SFs in 3C-SiC and has a selective role in the disclosing of 6H-like SF during the growth of 3C-SiC.[32,33] Despite the fact the SF density is reduced for increased doping levels, the average length of the remaining SFs increases. A similar effect was already observed during the growth series with various growth temperatures. One of the reduction mechanisms for the closure of SFs in (001)-oriented 3C-SiC is the annihilation of one SF if two defects converge. However, with a reduced SF density, the probability of this annihilation is reduced, leading to an expansion in size of the remaining SFs.[17] This effect is enhanced for the growth on 4° off axis material, as prolongation of SFs along $(-1-11)$ is generally suppressed based on the step flow orientation, reducing the probability of the coincidence of two defects.

While nitrogen proves to have a positive effect on the SF density, a slight broadening of the Raman TO mode could be observed for the higher doped samples in this study. The average FWHM of the TO mode increases from 4.1 ± 0.2 cm^{-1} for the lowest doped sample to 4.4 ± 0.3 cm^{-1} for the medium-doped sample, while the high-doped samples have values of 4.5 ± 0.3 and 5.8 ± 0.8 cm^{-1}, respectively. This observation seems to contradict the expected results, since a reduced SF density should lead to an increased layer quality and hence a sharper TO mode. However, it can be explained by the initial nucleation phase during CS-PVT and the penetration depth of the laser used for Raman measurements. During sublimation growth of 3C-SiC on homoepitaxial seeds an increase of SFs at the interface between the seed and the newly nucleated material can be observed, as shown by Schoeler et al.[19] This defective transition layer has a thickness of 50–100 μm. After the initial increase, the SF density starts to decrease and reaches values below the ones measured in the seeding layer. The initial increase of SFs is most likely caused by the difference of the N_2 concentration between the seed and the newly grown material. Steiner and Wellmann[34] have shown that an increased number of crystallographic defects, e.g., SFs and dislocations, will be formed during 4H-SiC growth, if the doping mismatch between seed and growing material is too high. In this context, the mismatch is caused by different lattice spacings for undoped and doped SiC. Nitrogen will be incorporated on a C-side, leading to a reduction of the lattice constant due to a smaller covalent radius of N than that of C and was also observed in 3C-SiC.[23]

The grown samples of the N_2 doping series in this study had the lowest overall thickness, with the CS-PVT grown layer being 340–380 μm thick. Meanwhile, the used laser for the Raman measurements ($\lambda = 532$ nm) is not surface sensitive but has a penetration depth of a few hundred micrometers. Consequently, during Raman measurements also information from the highly defective interface layer and the used seeds are obtainable in the spectrum. This leads, one the one hand, to the appearance of a second LO mode at a Raman shift of 972 cm^{-1}, which is correlated to the intrinsic seeding layer (see **Figure 9**a). On the other hand, the defective material of the transition layer broadens the measured TO mode based on the lower material quality (see Figure 9b). This effect is most pronounced for the highest doped sample, since the difference in the N_2 concentration is the largest compared to the intrinsic seeding layer. On the samples of the other two growth series (temperature and pressure variation) the described effect is not observable, since the grown layer are thicker
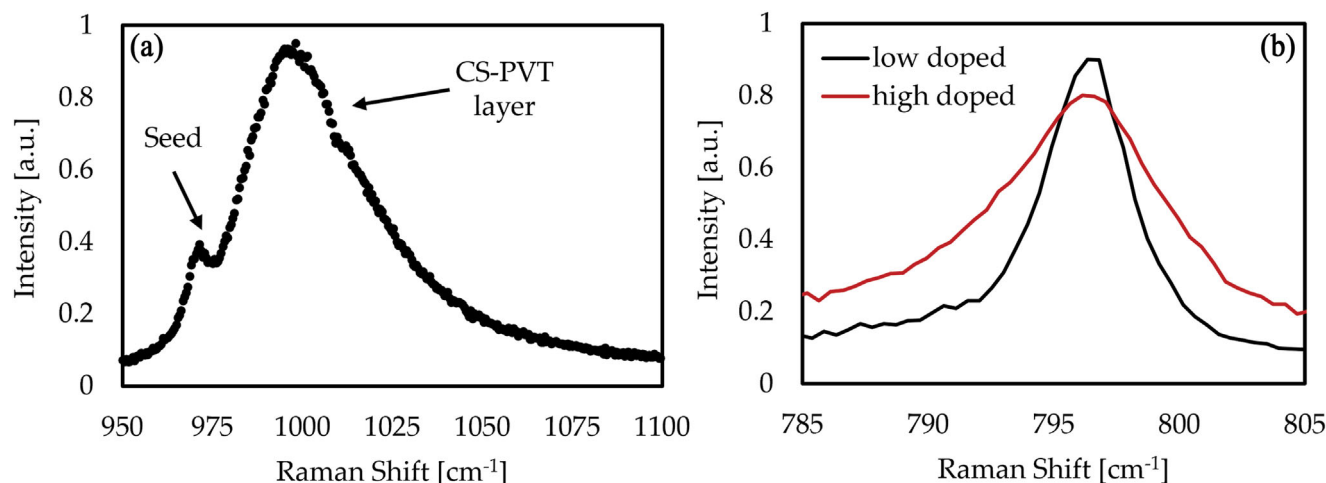
**ADVANCED
SCIENCE NEWS**

www.advancedsciencenews.com

CRYSTAL
Research&Technology

www.crt-journal.org

Figure 9. a) Raman spectrum of the LO mode for crystal E (growth series with focus in N_2 doping). Two LO modes are visible, one for the intrinsic seeding layer at 972 cm^{-1} and one for the CS-PVT grown material, shifted to higher wave numbers by the N_2 doping. The LO mode of the seed is visible since the penetration depth of the used laser reaches to the interface between seed and newly grown material. b) Raman TO mode for a low-doped (crystal A) and a high-doped (crystal G) sample. For the increased N_2 doping a broadening of the TO mode is visible based on the increase of the SF-density at the interface between seed and CS-PVT grown material.

and consequently only information from the CS-PVT material are detectable during Raman measurements.

4. Conclusion

Sublimation growth of 3C-SiC on homoepitaxial grown seeding layers was conducted using CS-PVT. Growth temperature, pressure, and N_2 doping were varied and the influence on the surface morphology and defect density was analyzed. Crystals with a smooth surface consisting of microsteps on an underlying macrostep structure could be grown for temperatures of 1960–1980 °C. The overall SF density compared to the seeding layers could be reduced for all growth runs while the average SF length increased. Partly, the formation of strongly bunched areas (macrobunching) at the surface was observed. Often SFs are detectable near the MBs indicating a correlation between the appearance of the defect and the macroscale bunching. At higher growth temperatures step bunching was enhanced leading to increased dimensions of the MBs. Higher growth pressures led to an enhanced incorporation of nitrogen as well as an enhanced step bunching. Similar to increased temperatures, no significant influence was found on the SF density. Nitrogen doping showed only a minor influence on the microscopic surface morphology. Meanwhile on macroscopic scale similar effects as for increased growth pressure and temperature could be observed. A correlation between increasing N_2 doping and a decreasing SF density could be identified while simultaneously an increase in the average length of SFs was detected. A broadening of the Raman TO mode could be seen with increasing N_2 doping, which is based on the formation of additional SFs at the interface between the seed and the growing crystal. While the difference in nitrogen concentrations between the seeding layer and the newly grown material leads to the initial high SF density, N_2 also showed a positive effect with respect to SF reduction during further sublimation growth. Depending on the target thickness of the grown

material, a compromise between these two effects needs to be found.

Conflict of Interest

The authors declare no conflict of interest.

Data Availability Statement

The data that support the findings of this study are available from the corresponding author upon reasonable request.

Author Contributions

Conceptualization: M.K. and P.W.; methodology: M.K and P.W.; software: M.K.; formal analysis: M.K.; investigation: M.K.; resources: F.L.V. and P.W.; writing—original draft preparation: M.K.; writing—review and editing: M.K., F.L.V., and P.J.W.; visualization: M.K.; supervision: F.L.V. and P.J.W.; project administration: F.L.V. and P.J.W.; and funding acquisition: F.L.V. and P.J.W. All authors have read and agreed to the published version of the manuscript.

[1] F. La Via, M. Zimbone, C. Bongiorno, A. La Magna, G. Fisicaro, I. Deretzis, V. Scuderi, C. Calabretta, F. Giannazzo, M. Zielinski, *Materials* **2021**, *14*, 5348.

[2] P. Wellmann, N. Ohtani, R. Rupp, *Wide Bandgap Semiconductors for Power Electronics: Materials, Devices, Applications*, John Wiley & Sons, Weinheim **2021**.

[3] M. Soueidan, G. Ferro, B. Nsouli, F. Cauwet, J. Dazord, G. Younes, Y. Monteil, *Mater. Sci. Eng., B* **2006**, *130*, 66.

[4] H. S. Kong, J. Glass, R. F. Davis, *J. Mater. Res.* **1989**, *4*, 204.

[5] P. G. Neudeck, A. J. Trunek, D. J. Spry, J. A. Powell, H. Du, M. Skowronski, X. R. Huang, M. Dudley, *Chem. Vap. Deposition* **2006**, *12*, 531.

[6] V. Jokubavicius, G. R. Yazdi, R. Liljedahl, I. G. Ivanov, J. Sun, X. Liu, P. Schuh, M. Wilhelm, P. Wellmann, R. Yakimova, *Cryst. Growth Des.* **2015**, *15*, 2940.

[7] M. Zielinski, S. Ndiaye, T. Chassagne, S. Juillaguet, R. Lewandowska, M. Portail, A. Leycuras, J. Camassel, *Phys. Status Solidi A* **2007**, *204*, 981.

[8] V. Cimalla, J. Pezoldt, O. Ambacher, *J. Phys. D: Appl. Phys.* **2007**, *40*, 6386.

[9] R. Anzalone, M. Zimbone, C. Calabretta, M. Mauceri, A. Alberti, R. Reitano, F. La Via, *Materials* **2019**, *12*, 3293.

[10] M. Schöler, F. La Via, M. Mauceri, P. Wellmann, *Cryst. Growth Des.* **2021**, *21*, 4046.

[11] M. Kollmuß, M. Mauceri, M. Roder, F. L. Via, P. J. Wellmann, *Rev. Adv. Mater. Sci.* **2022**, *61*, 829.

[12] S. Zoppel, M. Farsari, R. Merz, J. Zehetner, G. Stangl, G. A. Reider, C. Fotakis, *Microelectron. Eng.* **2006**, *83*, 1400.

[13] R. Anzalone, N. Frazzeto, F. La Via, (STMicroelectronics S.r.l.), *US 2021/0062361 A1*, **2021**.

[14] H. Yugami, S. Nakashima, A. Mitsuishi, A. Uemoto, M. Shigeta, K. Furukawa, A. Suzuki, S. Nakajima, *J. Appl. Phys.* **1987**, *61*, 354.

[15] S. A. Sakwe, Z. Herro, P. J. Wellmann, *Mater. Sci. Forum* **2005**, *483*, 283.

[16] P. Schuh, M. Schöler, M. Wilhelm, M. Syväjärvi, G. Litrico, F. La Via, M. Mauceri, P. Wellmann, *J. Cryst. Growth* **2017**, *478*, 159.

[17] F. La Via, A. Severino, R. Anzalone, C. Bongiorno, G. Litrico, M. Mauceri, M. Schoeler, P. Schuh, P. Wellmann, *Mater. Sci. Semicond. Process.* **2018**, *78*, 57.

[18] M. Camarda, A. La Magna, A. Severino, F. La Via, *Thin Solid Films* **2010**, *518*, S159.

[19] M. Schoeler, P. Schuh, G. Litrico, F. La Via, M. Mauceri, P. J. Wellmann, *Adv. Mater. Proc.* **2017**, *2*, 774.

[20] H. Nagasawa, K. Yagi, T. Kawahara, N. Hatta, *Chem. Vap. Deposition* **2006**, *12*, 502.

[21] D. Avrov, A. Bakin, S. Dorozhkin, V. Rastegaev, Y. M. Tairov, *J. Cryst. Growth* **1999**, *198*, 1011.

[22] N. Ohtani, M. Katsuno, J. Takahashi, H. Yashiro, M. Kanaya, *J. Appl. Phys.* **1998**, *83*, 4487.

[23] M. Zielinski, M. Portail, T. Chassagne, S. Juillaguet, H. Peyre, *J. Cryst. Growth* **2008**, *310*, 3174.

[24] M. Arzig, U. Künecke, M. Salamon, N. Uhlmann, P. J. Wellmann, *J. Cryst. Growth* **2021**, *576*, 126361.

[25] P. J. Wellmann, *Semicond. Sci. Technol.* **2018**, *33*, 103001.

[26] Q.-S. Chen, H. Zhang, V. Prasad, C. Balkas, N. Yushin, S. Wang, *J. Cryst. Growth* **2001**, *224*, 101.

[27] D. Avrov, S. Dorozhkin, Y. M. Tairov, A. Y. Fadeev, A. Lebedev, *Semiconductors* **2008**, *42*, 1469.

[28] D. J. Larkin, P. G. Neudeck, J. A. Powell, L. G. Matus, *Appl. Phys. Lett.* **1994**, *65*, 1659.

[29] N. Ohtani, M. Katsuno, T. Aigo, T. Fujimoto, H. Tsuge, H. Yashiro, M. Kanaya, *J. Cryst. Growth* **2000**, *210*, 613.

[30] W. Chen, K.-y. Lee, M. A. Capano, *J. Cryst. Growth* **2006**, *297*, 265.

[31] C. Calabretta, V. Scuderi, R. Anzalone, M. Mauceri, D. Crippa, A. Cannizzaro, S. Boninelli, F. La Via, *Materials* **2021**, *14*, 4400.

[32] C. Calabretta, V. Scuderi, C. Bongiorno, A. Cannizzaro, R. Anzalone, L. Calcagno, M. Mauceri, D. Crippa, S. Boninelli, F. La Via, *Cryst. Growth Des.* **2022**, *22*, 4996.

[33] Y. Umeno, K. Yagi, H. Nagasawa, *Phys. Status Solidi B* **2012**, *249*, 1229.

[34] J. Steiner, P. J. Wellmann, *Materials* **2022**, *15*, 1897.